

The effect of ruthenium promotion of the $\text{Co}/\delta\text{-Al}_2\text{O}_3$ catalyst on the hydrogen reduction kinetics of cobalt

Olga A. Kungurova^{1,2,3} · Natalya V. Shtertser² ·
Egor G. Koemets^{1,2} · Svetlana V. Cherepanova^{1,2} ·
Alexander A. Khassin^{1,2}

Received: 30 September 2016 / Accepted: 2 December 2016 / Published online: 16 December 2016
© Akadémiai Kiadó, Budapest, Hungary 2016

Abstract The effect of ruthenium content on the reductive activation of the $\text{Co}/\delta\text{-Al}_2\text{O}_3$ catalyst was investigated using thermal analysis and in situ synchrotron radiation X-ray diffraction. Data of thermal analysis and phase transformations can be described by a kinetic scheme consisting of three sequential steps: $\text{Co}^{3+} \rightarrow \text{Co}^{2+} \rightarrow (\text{Co}^0\text{Co}^{2+}) \rightarrow \text{Co}^0$. The first step is the generation of several CoO clusters within one Co_3O_4 crystallite followed by their further growth obeying the Avrami–Erofeev kinetic equation (An_1) with dimensional parameter $n_1 < 1$, which may indicate the diffusion control of the growth. The second step is the kinetically controlled sequential process of the metallic cobalt phase nucleation (An_2), which is followed by the third step of slow particle growth limited by mass transport according to the Jander model (D). Ruthenium promotion of $\text{Co}/\delta\text{-Al}_2\text{O}_3$ catalysts significantly accelerates the reduction of cobalt. As the ruthenium content is raised to 1 wt%, the characteristic temperature of metal phase formation decreases by more than 200 °C and E_a for An_2 step decreases by 25%. For step D, a joint decrease in activation energy and pre-exponential factor in case of ruthenium promotion corresponds to a weaker diffusion impediment at the final step of cobalt reduction. In the case of unmodified $\text{Co}/\delta\text{-Al}_2\text{O}_3$, the characteristic temperature of the metal phase formation reaches very high values, the metallic nuclei rapidly coalesce into larger ones, and the further process is inhibited by diffusion of the reactants through the product layer. For ruthenium promoted catalysts, each CoO crystallite generates one metal crystallite; thus, ruthenium enhances the dispersion of the active component.

✉ Olga A. Kungurova
olya-sky@inbox.ru

¹ Novosibirsk National Research University, 2, Pirogova Str., Novosibirsk, Russia 630090

² Boreskov Institute of Catalysis, 5, Lavrentieva Ave., Novosibirsk, Russia 630090

³ Tomsk State University, 36, Lenina Ave., Tomsk, Russia 634050

Keywords Cobalt–alumina catalysts · Promotion · Ruthenium · Reduction · Kinetics · Mechanism

Introduction

Active catalytic sites of supported cobalt catalysts for Fischer–Tropsch synthesis (FTS) are represented by the metallic cobalt nanoparticles obtained by the reduction of oxide precursors in a flow of hydrogen-containing mixture or syngas. The reduction of Co_3O_4 cobalt oxide and cobalt-containing catalysts was studied by structural methods (in situ XRD and in situ EXAFS/XANES) using temperature-programmed heating [1–4]. It was found that the reduction of bulk Co_3O_4 and any supported cobalt catalyst consists of two steps: (1) the reduction of Co^{3+} cations to Co^{2+} accompanied by the phase transformation $\text{Co}_3\text{O}_4^* \rightarrow \text{CoO}^*$ (hereinafter, an asterisk indicates the possible presence of impurity anions and cations of the support or promoter in the phase composition), and (2) the reduction of Co^{2+} cations to metallic cobalt, $\text{CoO}^* \rightarrow \text{Co}$. Depending on the cationic and anionic composition of the initial oxide, its dispersion, degree of interaction with the support, and conditions of experiment (heating rate and partial pressure of hydrogen), the phases may have strongly different temperature regions of existence and final sizes of metallic particles [5–7]. Thus, in the case of the cobalt-containing systems supported on alumina, the spinel-like Co_3O_4^* phase may comprise Al^{3+} cations: $\text{Co}_{3-x}\text{Al}_x\text{O}_4$ ($0 \leq x \leq 2$), and high degree of reduction to metallic state will require high activation temperatures. This feature is common for all Co–Al catalysts: thermal conversion of the supported precursors (salts, hydroxides, double hydroxides) of cobalt is accompanied by the interaction of cobalt cations with the support or the formation of cobalt–aluminum double oxides from mixed Co and Al precursor compounds (for example, upon the decomposition of double hydroxocarbonates with a hydroxalcite-type structure) [8, 9]. As a consequence, the formation of catalytically active sites via the reduction of cobalt cations from double oxides in a flowing hydrogen-containing mixture occurs at a temperature of 500–600 °C and a hydrogen pressure of 0.1–1 atm [1, 3, 10]. However, even at such a high temperature, not all cobalt cations are reduced to the metallic state. On the other hand, some metal–support interaction is desirable because it increases dispersion of the particles due to anchoring of the active component, prevents migration and sintering, and thus ensures high activity of the catalyst and its stability [11–13].

A possible way to lower the activation temperature of cobalt-containing catalysts is the introduction of noble metals, in particular Pt, Pd, Ru or Re. They promote the reduction of cobalt to metallic state. However, platinum and palladium adversely affect its selectivity and exhibit their proper activity in the hydrogenation of CO to methane and light hydrocarbons [14, 15]. At the same time, the introduction of up to 5 wt% of ruthenium decreases only slightly or even increases the selectivity of cobalt-containing catalysts for high-molecular hydrocarbons. Several research teams demonstrated that the promotion of Co– Al_2O_3 catalysts with small amounts

of ruthenium decreases the characteristic temperature of cobalt reduction by 100–150 °C (according to TPR data) and increases the dispersion by a factor of 2 or more (according to hydrogen chemisorption followed by titration with oxygen) [14–20]. In [21], hydrogen chemisorption did not show an increase in the dispersion after the promotion of cobalt catalyst. However, the scanning electron microscopy study revealed that the fraction of ultradisperse particles (smaller than 6 nm) decreased from 83 to 49%, while the fraction of 6–12 nm particles (the size optimal for FTS), accordingly, increased from 17 to 51%.

At least two mechanisms underlying the effect of a noble metal Nm in the promoted catalysts on the reduction process were proposed. The first mechanism (hydrogen spillover effect) implies that a noble metal serves as the hydrogen activation site, which is then transported to cobalt oxide over the support surface [22–24]. In this case, the effect of the promoter metal can show up even in the absence of direct contact between Nm and Co. According to the second mechanism, the effect of Nm on cobalt reduction includes the formation of mixed Co–Nm compounds during the preparation (synthesis and thermal treatment), the reduction temperature of which is lower as compared to the precursor of monometallic Co particles [14, 25–27]. For example, the authors of [26] noted that the oxidative pretreatment at temperatures above 327 °C is a necessary condition for the formation of precursors of bimetallic Co–Ru particles in the Co–Ru–TiO₂ catalyst. Precursors of the bimetallic particles and their reduction were investigated in [4, 14]. It was found that 0.2 wt% Nm (Pd, Pt, Ru) in the composition of Co–SiO₂ catalyst can form highly disperse particles of a metallic alloy with Co upon reduction. Segregation of intermetallic Co–Ru particles with ruthenium enrichment of the surface was observed in [14]. The formation of bimetallic particles can explain the observed effect on the catalytic characteristics: the FTS activity of the catalysts pre-reduced under similar conditions decreases in the series RuCo–SiO₂ > PdCo–SiO₂ > PtCo–SiO₂ > Co–SiO₂. In [4], the structure of cobalt and ruthenium compounds in the Ru–Co/SiO₂ catalyst, which are formed upon calcination and reduction, was investigated by means of time-resolved in situ X-ray absorption spectroscopy. It was found that upon reductive calcination, Ru⁴⁺ cations are inserted inside Co₃O₄ nanoparticles. The reduction of the oxidic phase takes place in two distinct steps at approximately the same temperatures regardless of the ruthenium content: first to Ru³⁺-containing CoO nanoparticles (Ru ions modifying the intrinsic electronic properties of the oxidic nanoparticles), and then to bimetallic Co nanoparticles containing Ru⁰ atoms, via an autocatalytic process. It should be noted also that, according to the listed studies, the promotion of catalysts with Nm facilitates mostly the second-step reduction, CoO → Co. For example, in [25] the contribution of Pt to Co–Al₂O₃ reduction is supposedly related to an increase in the fraction of cobalt that was reduced from the small CoO particles strongly interacting with the support.

In the present work, the effect of small amounts of ruthenium compounds introduced into the cobalt–alumina catalyst on the phase composition, kinetics and mechanism of reduction under non-isothermal conditions was studied using thermal analysis and in situ XRD.

Experimental and/or theoretical methods

Catalyst synthesis

The cobalt–alumina catalyst denoted as CoAl was synthesized using deposition by precipitation under the conditions of urea hydrolysis (deposition by precipitation with urea, DPU) [3, 28, 29] at a temperature of 90 °C for 5 h. The synthesis was performed with δ -Al₂O₃, which was obtained by heat treatment of granulated pseudoboehmite extrudate A-64 (diameter 3 mm, length 4–5 mm, JSC Angarsk Catalysts and Organic Synthesis Plant) in air at 900 °C for 3 h, and solutions of 3 M Co(NO₃)₂ (pure, GOST 4528-78) and 10.8 M urea (analytically pure, GOST 6691-77). Upon completion of the synthesis, catalyst granules were separated from the resulting suspension of disperse Co–Al hydroxocompound, carefully washed with distilled water and dried in air. Dry precursors of the cobalt catalyst are cobalt–aluminum hydroxo-nitrate–carbonates with a hydrotalcite-like structure, where the content of anions depends on the concentrations of working solutions of cobalt nitrate, aluminum and urea [3, 29].

It was shown in [30] that so prepared catalytic precursors contain at least two phases of (i) alumina and (ii) layered double hydroxide (LDH) with hydrotalcite-like structure; the latter originates from the interaction of Co cations with alumina. Hydrotalcite-like LDH decomposes upon the calcination of the precursor giving spinel-like mixed cobalt–aluminum oxide, which is as well supported by alumina. In order to clarify the effect of the alumina support on the process of cobalt reduction, we have synthesized the unsupported model sample CoAl–M by co-precipitation of Co²⁺ and Al³⁺ (Co:Al = 4 at.) from 10% solutions of their nitrates with a sodium carbonate solution at pH 7.1–7.2 and a temperature of 68–70 °C. According to X-ray diffraction data, the model sample is the single phase of Co²⁺–Al³⁺ LDH with hydrotalcite-type structure after drying. Refined lattice parameters are $a = 3.08(1)$ Å, $c = 22.86(1)$ Å. The mean coherent scattering region (CSR) sizes are estimated as $\langle L_a \rangle = 25$ nm, $\langle L_c \rangle = 8$ nm.

All samples were dried at 50 °C for 24 h under an IR lamp and then calcined: the CoAl catalyst at 350 °C for 1.5 h in flow of Ar and the model CoAl–M sample at 500 °C for 5 h in flow of air. After calcination, the model CoAl–M sample consists of the single phase of spinel-like oxide; the supposed composition of the oxide is Co²⁺(Co_{1.4}Al_{0.6})³⁺O₄, while the other catalysts under the study were mixtures of two phases: Co₃O₄^{*}, which has the spinel-like structure and δ -Al₂O₃ having the defect spinel structure.

Ruthenium promoted catalysts were prepared by the incipient wetness impregnation of dry CoAl catalyst granules with aqueous solutions of *trans*-Ru(NO)(NH₃)₂(NO₃)₃ complex [31] followed by drying at 50 °C in air for 12 h. The promoted catalysts are denoted as CoRu(*x*)Al, where $x = 0.2, 0.5$ or 1.0 is the target content of ruthenium (wt%) in the promoted catalyst. The cobalt content in all dry precursors of CoRu(*x*)Al catalysts varies from 9.1 to 9.4 wt% and corresponds to the cobalt content of the initial catalyst. The Ru content in the modified dry samples is by 6–10% lower than the theoretical value; this can be related to the

presence of impurity anions and water that are not taken into account by theoretical estimates. Calcination of the precursors in flowing argon up to 350 °C at a rate of 2 °C/min produced a 14–15% weight loss. Thus, the cobalt content in CoAl and CoRu(*x*)Al oxide catalysts is 10.5–10.9 wt% (data on the elemental content are listed in Table 1).

Bulk Co₃O₄, which was used as the reference sample, was obtained by calcination of cobalt carbonate in air at 600 °C for 3 h.

X-ray diffraction study

In situ XRD experiments were carried out at the Siberian Synchrotron and Terahertz Radiation Center, Novosibirsk, Russian Federation, on an X-ray powder diffractometer mounted on SR Beamline No.6 of VEPP-3 electron storage ring. The diffractometer consists of monochromator, set of beam collimating slits and position-sensitive X-ray detector. The Ge(111) or Si(111) crystal acting as a single reflection monochromator deflects the monochromatic beam upward at ~30° and provides the monochromaticity of ~ $(2-3) \times 10^{-4}$. The operation wavelength is 1.731 or 1.643 Å. The parallax-free position-sensitive detector OD-3M-350 produced by Budker Institute of Nuclear Physics, Novosibirsk, Russian Federation, collects X-ray diffraction patterns within angular range of about 30° with a resolution of ~0.01°.

The diffractometer is equipped with an X-ray high temperature reaction chamber XRK-900 (Anton Paar, Austria) allowing the experiments under non-ambient conditions in oxidation/reduction/inert atmosphere and high temperature up to 900 °C. The sample is loaded into the open sample holder, which permits the reaction mixture to pass through the powder sample, and is mounted in the reaction chamber.

The reduction was performed in hydrogen generated by a Varian Aerograph 9225 water electrolyzer. Hydrogen was subjected to a two-step desiccation in columns with silica gel as the humidity indicator. The gas flow rate was 15 cm³_{STP}/min. X-ray diffraction patterns were recorded each minute within the 2θ angular range of

Table 1 Elemental composition, lattice parameters of cobalt-containing phases, and weight losses of cobalt–alumina catalysts

Catalyst	Content in calcined sample, wt%		Lattice parameters of phases, Å			Weight loss upon reduction, %	
	Co	Ru	Co ₃ O ₄ * (30 °C)	CoO* (273 °C)	Co ⁰ (570 °C)	Step 1	Step 2 ^a
CoAl–M	45.4	–	8.09	4.24	3.60	6.1	17.9
CoAl	10.9	–	8.07	4.26	3.58	2.0	4.5
CoRu(0.2)Al	10.6	0.21	8.07	4.25	3.58	1.8	4.8
CoRu(0.5)Al	10.5	0.52	–	–	–	1.7	4.9
CoRu(1.0)Al	10.8	1.08	8.07	4.23	3.58	1.5	5.4

^a Up to 900 °C

31–58° with an exposure time of 1 min/frame. The heating rate was 3 °C/min. XRD patterns of the support were recorded upon heating in air at 3 °C/min to 700 °C.

Processing of experimental data

Since the support phase δ -Al₂O₃, which is present in the catalysts, has defects, its structure cannot be refined by the Rietveld method in a perfect crystal approximation. So, this phase was accounted for as the “*hkl* phase”. X-ray diffraction patterns of the support, which were taken in a wide temperature range similar to the patterns of catalysts, were used to determine unit cell parameters of the support (symmetry space group P4₁2₁2) as well as the intensity ratio of peaks by the Le Bail method [32].

Peaks of the deposited component and support phases were separated in a zero approximation under the assumption that the structure of support does not change after deposition of the active component, drying and calcination (before the reduction). So, the intensity ratio and shape of peaks (the peak widths and the ratio of Lorentzian and Gaussian functions in pseudo-Voigt function chosen to describe the peaks) of the support were fixed. At the same time, unit cell parameters of the support were refined because they changed due to thermal expansion. At higher temperatures (the reduction to metallic cobalt), a new refinement of the *hkl* phase of the support was made, i.e. a new intensity ratio and shape of the peaks were determined by the Le Bail method. Peaks of the support and metallic cobalt overlap only slightly, so the data obtained for the support phase are quite correct. Within the temperature region of existence of the CoO phase, the second (high-temperature) set of data for the support was taken as a base with possible small deviations.

Lattice parameters, average sizes of coherent scattering region (CSR), and weight fractions of all supported phases were found by the Rietveld method in TOPAS software (Bruker, Germany) with simultaneous refinement of parameters for the *hkl* phase of the support. The mean size of the error of CSR is 10% for intervals of the existence of a single phase; in cases where two phases coexist—20%.

Thermal analysis

The reduction kinetics of cobalt catalysts was investigated by thermal analysis; thermogravimetry curves (TG and DTG) were recorded on a Netzsch STA 409 PC Luxx instrument. The measurements were made with the use of Pt–Ir crucibles. A 100-mg powdered sample was used in the study. Thermal curves of the samples were recorded in a range from 50 to 900 °C at heating rates of 3, 6 and 12 °C/min in a mixture of argon and hydrogen. A 20 cm³_{STP}/min hydrogen flow was mixed with a 20 cm³_{STP}/min flow of shielding gas (argon) from balance. The total gas flow around the sample was 40 cm³_{STP}/min with a molar ratio of H₂:Ar = 1. To take into account the buoyancy (the Archimedian force and viscous friction of the gas flow), each measurement of the reduction kinetics of catalysts was preceded by determination of the correction curve: TG and DTG curves of corundum were recorded using the same weight of the sample, the same heating rate, crucible and

atmosphere. To estimate the effect of heat and mass transfer, a series of the same experiments was carried out with a smaller (20 mg) sample of CoAl catalyst. The reduction kinetics of individual Co_3O_4 oxide was studied for comparison purposes.

The Netzsch Kinetic 3 program package was employed for selection of kinetic models, calculation of kinetic parameters, and description of kinetics by the Friedman and Ozawa–Flynn–Wall model free methods.

Results and discussion

Evolution of the phase composition and structure of catalysts during non-isothermal reduction

Fig. 1 displays experimental DTG profiles for the reduction of model sample and catalysts in dependence on temperature at three heating rates.

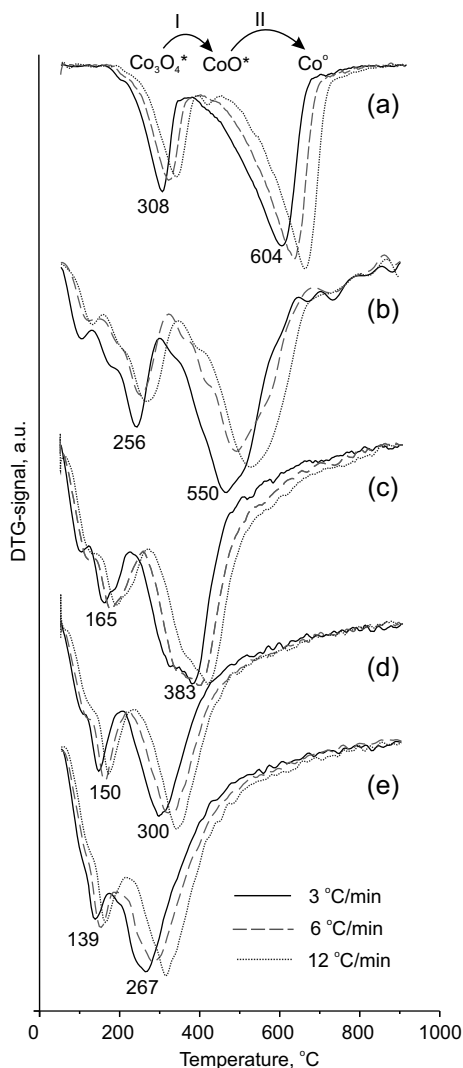
For all the samples, cobalt reduction from the oxide precursors to Co^0 occurs in two main steps associated with weight losses. Weight losses of the samples and data on their elemental composition are listed in Table 1. Fig. 2 displays the X-ray diffraction patterns for CoAl–M, CoAl, CoRu(0.2)Al and CoRu(1.0)Al obtained in situ upon reduction in a 100% hydrogen medium at a heating rate of 3 °C/min.

The model sample CoAl–M is the single phase of Co–Al mixed oxide with spinel like structure, $a = 8.09 \text{ \AA}$. The initial structure of the catalysts is a mixture of two phases: Co_3O_4^* , which has the spinel-like structure with the lattice parameter of ca. 8.07 Å, and $\delta\text{-Al}_2\text{O}_3$ having the defective spinel structure, lattice parameters $a = 7.96 \text{ \AA}$ and $c = 23.4 \text{ \AA}$, and the average SCR size of the support phase equal to 8.4 nm. The Co_3O_4^* phase may comprise also aluminum cations; X-ray diffraction data cannot be used to determine the amount of aluminum in the spinel-like phase because Co_3O_4 oxide and Co–Al oxides of different composition (CoAl_2O_4 , Co_2AlO_4 , $\text{Co}_x\text{Al}_y\text{O}_{4-z}$) are known to have very close lattice parameters, 8.06–8.10 Å.

The processes accompanying the treatment of unmodified calcined CoAl catalyst can be conventionally divided into two main steps, which are denoted in Fig. 1 as I ($\text{Co}_3\text{O}_4^* \rightarrow \text{CoO}^*$) and II ($\text{CoO}^* \rightarrow \text{Co}^0$).

The preceding low-temperature effect of ca. 0.6 wt% weight loss in the temperature region below 200 °C corresponds to the removal of impurity anions and water: no significant changes are seen on X-ray diffraction patterns in this temperature region. It should be noted that the removal of impurity anions is incomplete in the indicated temperature region: thermal analysis data testify that a considerable part of impurity anions is removed from the sample at elevated temperatures upon reduction of cobalt cations. Indeed, even a complete reduction of 11 wt% cobalt to the metal from Co_3O_4 oxide should be accompanied by only a 4 wt% weight loss of the sample, but the actual weight loss upon heating in a hydrogen flow up to 900 °C is greater by 2.5–2.8 wt%. The greater weight loss may be caused also by a nonstoichiometric composition of the oxide: according to magnetic susceptibility data [10], in the Co–Al (1:1 at.) catalyst synthesized by coprecipitation and calcination in flowing inert gas at 450 °C, the fraction of Co^{3+}

Fig. 1 DTG profiles for the reduction of alumina supported cobalt catalysts in a range from 50 to 900 °C: (a) CoAl–M, (b) CoAl, (c) CoRu(0.2)Al, (d) CoRu(0.5)Al, (e) CoRu(1.0)Al at heating rates 3, 6 and 12 °C/min in a mixture of 50% Ar/50%H₂. Labels indicate the maximum rates of weight change at a heating rate of 3 °C/min



cations constituted 42% of the total cobalt content in the oxide. The superstoichiometric content of trivalent cobalt can be responsible for the greater weight loss of the sample upon reduction. However, this is only a partial explanation even if the entire cobalt is supposedly in the Co^{3+} state. In this connection, the greater weight loss upon reduction reliably indicates the removal of impurity ions (OH^- , CO_3^{2-} , NO_3^-). Ruthenium promotion does not exert a substantial effect on the weight loss during the catalyst reduction. Some redistribution of the weight loss from the first step to the second one is caused by shifting of the second step temperature range toward lower values and by a worse resolution of the observed processes. Note that the weight loss upon reduction of the model CoAl–M sample (24 wt%) is close to the theoretical value estimated from the stoichiometry of Co_3O_4 oxide (23.5 wt%).

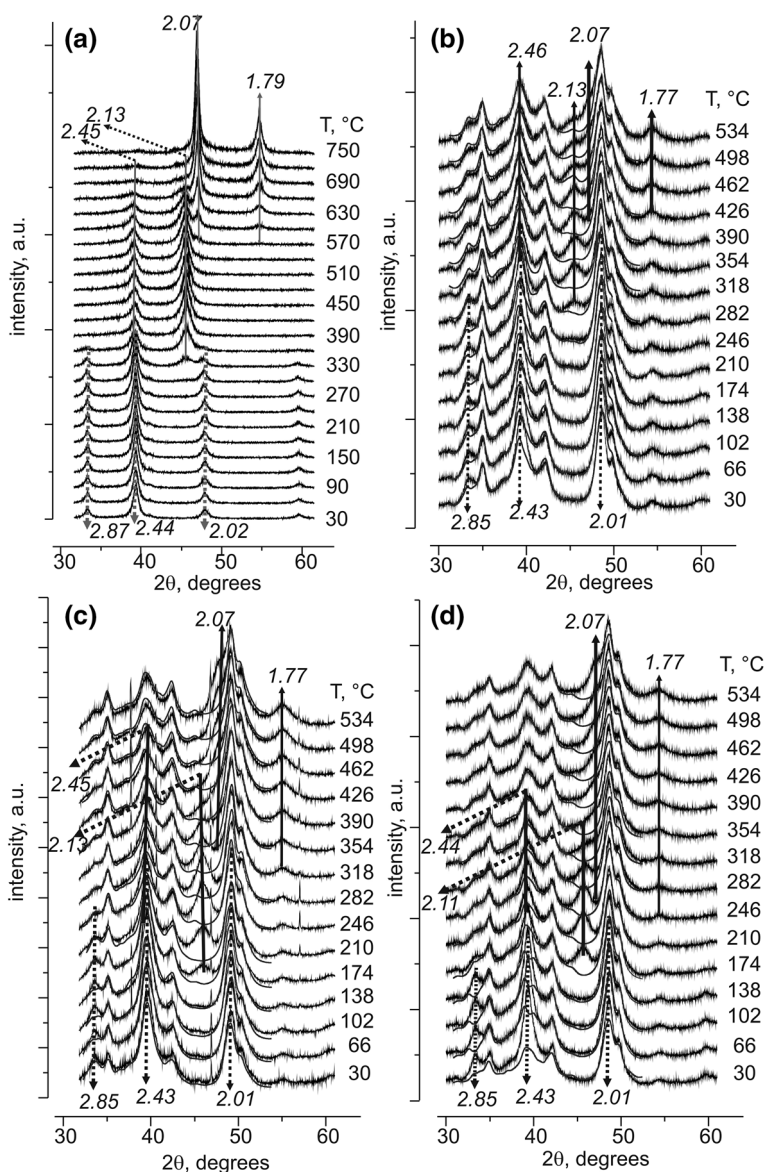


Fig. 2 X-ray diffraction patterns taking into account the support phase (solid line under XRD patterns) for CoAl–M (a), CoAl (b), CoRu(0.2)Al (c), and CoRu(1.0)Al (d), which were obtained in situ upon reduction in 100% hydrogen at a heating rate of 3 °C/min. Arrows indicate the temperature region of presence of cobalt phases. Numerals denote interplanar distances, Å

In the temperature range of 180–400 °C, XRD patterns of the CoAl sample show a decrease in the intensity of diffraction maxima with interplanar distances 2.8, 2.4 and 2.0 Å, which are typical of the Co_3O_4 * spinel-like structure (PDF#421467, $d_{220} = 2.8580$ Å, $d_{311} = 2.4370$ Å, $d_{400} = 2.0210$ Å), and the appearance of

diffraction maxima with interplanar distances 2.4 and 2.1 Å, which are typical of the CoO* structure (PDF#431004, $d_{111} = 2.4595$ Å, $d_{200} = 2.1300$ Å). This temperature range with $T_{\max} = 256$ °C, which is denoted in Fig. 1 as (I), corresponds to the reduction of Co^{3+} cations in cobalt-containing oxides to Co^{2+} . The CoO* phase obtained at this step has the NaCl-type structure. Despite of thermal expansion, the lattice parameter in the temperature region of 200–400 °C is equal to that of CoO at room temperature, $a = 4.26$ Å (PDF#431004). A possible reason is that CoO* contains quite a large number of Al^{3+} ions, the ionic radius of which ($r = 0.54$ Å in an octahedral environment) is smaller as compared to that of Co^{2+} cations ($r = 0.65$ Å).

The next reduction step is characterized by the disappearance of the CoO* phase and formation of the metallic cobalt phase with a defect structure, which is represented by alternating domains with fcc and hcp structures. The microdomain structure manifests itself by the presence of both fcc (PDF#150806, $d_{111} = 2.0467$ Å, $d_{200} = 1.7723$ Å) and hcp (PDF#050727, $d_{100} = 2.1650$ Å, $d_{002} = 2.0230$ Å, $d_{101} = 1.9100$ Å) reflections slightly shifted to lower angles. Therewith, the 111_{fcc} peak is much narrower than the 200_{fcc} peak, which in addition is shifted to lower diffraction angles. An additional broadening of the 200_{fcc} peak is caused by a small thickness of domains with fcc packing in metallic cobalt particles. So, lattice parameters were determined using only the peak with the interplanar distance $d = 2.07$ Å corresponding to 111_{fcc} and 002_{hcp} peaks (the distance between close packed layers in both structures). The calculated interplanar distance d_{630} °C = 2.07 Å is higher than tabular values for interplanar distances d_{111} (fcc) and d_{002} (hcp); this is caused by thermal expansion: estimation from $d_{111} = 2.047$ Å (PDF #150806) and $\alpha_L = 13 \times 10^{-6} \text{ K}^{-1}$ gives at 630 °C the value of $d_{111} = 2.06$ Å, which is equal to the experimental value within the accuracy of the analysis.

For the CoAl catalyst, the formation of metallic cobalt proceeds in a wider temperature range, from 400 to 600 °C, with a maximum weight loss at 550 °C. At temperatures above 600 °C, the reduction of cobalt aluminates with a high aluminum content takes place; this process may terminate at temperatures above 1000 °C.

For the model CoAl–M system, the characteristic temperatures of reduction steps and the temperature regions of existence of phases are by ca. 50 °C higher as compared to the CoAl catalyst. The higher reduction temperature may be caused by the formation of a better crystallized cobalt–aluminum spinel at a higher treatment temperature (500 °C). Lattice parameters of all the phases are close to the corresponding values for the CoAl catalyst.

The introduction of ruthenium precursor into the cobalt–alumina catalyst shifts the temperatures of both reduction steps, $\text{Co}_3\text{O}_4^* \rightarrow \text{CoO}^* \rightarrow \text{Co}$, to lower values. The dependence of T_{\max} shift on the content of introduced ruthenium is less pronounced at the first step of reduction: $T_{\max 1}$ decreases by ca. 100 °C for all the promoted samples, and more pronounced at the second step: as the Ru content is raised to 1 wt%, $T_{\max 2}$ decreases by more than 250 °C. The lattice parameters of all the phases are close to the corresponding values of the model and CoAl samples.

Model free analysis of the hydrogen reduction kinetics of cobalt–alumina catalysts upon temperature elevation

The calculation of kinetic parameters from TG curve is based on the following formal kinetic equation:

$$\frac{d\alpha}{dt} = \beta \frac{d\alpha}{dT} = k(T)f(\alpha) = A \exp\left(-\frac{E_a}{RT}\right)f(\alpha) \tag{1}$$

Here α is the degree of process completion, t is the time, T is the temperature, β is the heating rate (K/min), $f(\alpha)$ is the kinetic model, $k(T)$ is the rate constant that depends on temperature according to the Arrhenius equation with parameters A (pre-exponential factor) and E_a (activation energy), and R is the universal gas constant.

In the case of the model method, parameters of the theoretical model are chosen so as to ensure the better description of the experimental $d\alpha/dt$ dependence. In such approximation, the analytical dependence $d\alpha/dt = k(T) \cdot f(\alpha)$ is specified, and numerical nonlinear regression methods are employed to choose the optimal kinetic parameters.

In the case of the complex processes comprising several sequential–parallel steps, isoconversional methods are appropriate: the Friedman isoconversional differential method [33] and the Ozawa–Flynn–Wall isoconversional integral method [34, 35]. Isoconversional methods make it possible to obtain dependences of the apparent activation energy on the process depth irrespective of the process mechanism and $f(\alpha)$ function characterizing the process.

If the Friedman method is employed, Eq. 1 takes the following form:

$$\ln\left(\beta \frac{d\alpha}{dT_\alpha}\right) = \ln\{A_\alpha f(\alpha)\} - \frac{E_a}{RT} \tag{2}$$

Since $f(\alpha)$ is constant at any fixed α value, the dependence of the logarithm of conversion rate $d\alpha/dt$ for each heating rate β on $1/T_\alpha$ is the line with the slope equal to E_a/R , and its y-intercept is equal to $\ln\{A_\alpha f(\alpha)\}$. The pre-exponential factor is commonly assessed using the Arrhenius equation under the assumption of the first order reaction $f(\alpha) = (1 - \alpha)$ with averaging over all dynamic heating rates.

The Ozawa–Flynn–Wall method employs the following integral equation:

$$\ln \beta = -1.052 \frac{E_a}{RT_\alpha} + 5.3305 - \ln \left\{ \frac{R}{AE_a} \int_0^1 \frac{d\alpha}{f(\alpha)} \right\} \tag{3}$$

For the data obtained by a series of measurements with different heating rates β at a fixed conversion α , according to Eq. 3, the dependence of $\ln(\beta)$ on $1/T_\alpha$ will be the line with the slope equal to $-1.052 E_a/R$.

The kinetic study of solid-phase reduction of the catalysts under consideration and bulk Co_3O_4 was based on the Friedman and Ozawa–Flynn–Wall model free

approaches. Results of the study are presented as dependences of the apparent activation energies on the process depth (Fig. 3).

As seen on the energy profiles obtained by both methods, a complete reduction of the model system and supported catalysts starts from the reactions with lower E_a values and proceeds by the reaction route with a non-uniform growth of E_a , which testifies that the process consists of several steps.

The apparent activation energies of bulk cobalt oxide are much lower as compared to all the cobalt–alumina catalysts examined in our work. At a maximum reduction rate of bulk Co_3O_4 , the E_a values for the first and second steps were

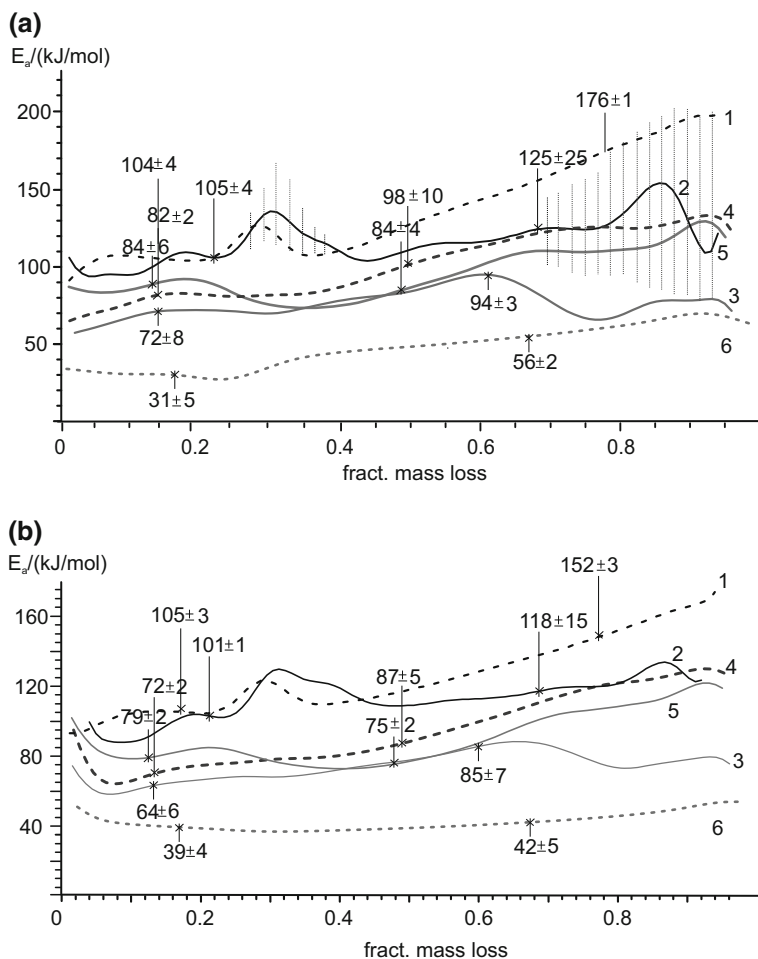


Fig. 3 Dependences of the apparent activation energies on the reduction process depth of alumina supported cobalt catalysts obtained by **a** Friedman and **b** Ozawa–Flynn–Wall methods: 1—CoAl–M, 2—CoAl, 3—CoRu(0.2)Al, 4—CoRu(0.5)Al, 5—CoRu(1.0)Al, 6— Co_3O_4 . Numerical labels correspond to E_a values at the sites of maximum conversion rate (T_{\max} on DTG curves obtained in a range from 50 to 900 °C at heating rates 3, 6 and 12 °C/min in a mixture of 50% Ar/50% H_2), vertical dotted lines on the Friedman profiles indicate the accuracy of the method for CoAl

31 ± 5 and 56 ± 2 kJ/mol by the Friedman method and 39 ± 4 and 42 ± 5 kJ/mol by the Ozawa–Flynn–Wall method. The introduction of aluminum into the oxide composition (CoAl–M model sample and CoAl catalyst) produces a sharp increase in the apparent values of activation energy. For the CoAl catalyst, at the sites of maximum conversion rate $E_a^{(I)}(\alpha_{\max} \approx 0.2)$ reaches 102 ± 10 (Friedman) and 97 ± 3 (Ozawa–Flynn–Wall) kJ/mol, and $E_a^{(II)}(\alpha_{\max} \approx 0.7)$ is 125 ± 25 and 118 ± 15 kJ/mol, respectively. Profiles of the model CoAl–M sample and CoAl catalyst coincide at the first step. However, the second step is characterized by a monotonic growth of apparent activation energy for the model sample, which may be caused by a monotonic increase in the aluminum content of the mixed oxide accompanying the reduction of cobalt and its transition from the oxide to the metallic phase. The maximum at $\alpha \approx 0.3$, i.e. in the region of a drastic change of the process rate between two steps, seems to be an artefact caused by an error in determination of conversion α . In the case of the ruthenium promoted samples, this error did not produce such an artefact because steps (I) and (II) are less resolved.

The apparent activation energies of all Ru-modified samples are much lower, and the Friedman and Ozawa–Flynn–Wall profiles are similar within the accuracy of the method. The maximum conversion rate at the first reduction step slightly shifts toward lower conversions with a decrease in E_a by ca. 30%, while the maximum rate of the second step shifts considerably with a decrease in E_a by ca. 40%. At $\alpha > 0.65$, E_a values for the CoRu(0.2)Al catalyst are much lower as compared to the catalysts having a greater amount of ruthenium and, in distinction to them, the activation energy does not increase in the course of reduction.

Modeling of the hydrogen reduction kinetics of cobalt–alumina catalysts upon temperature elevation using regression analysis methods

To analyze the possible reduction mechanism of cobalt, experimental kinetic dependences $d\alpha/dt$ were simulated by regression analysis methods. Models were fitted to experimental TG curves for the CoAl catalyst with exclusion of the first effect, whose weight loss constitutes ca. 0.6% (Fig. 4). The corresponding value of the apparent activation energy obtained by model free methods was chosen as the initial value of activation energy for each step.

As the reduction of CoAl, CoRu(x)Al catalysts consists at least of two consecutive reactions $\text{Co}_3\text{O}_4^* \rightarrow \text{CoO}^*$ and $\text{CoO}^* \rightarrow \text{Co}^0$, the primary search for models was performed for the two-step kinetic scheme $A \rightarrow B \rightarrow C$. The search for models to the indicated mechanism has revealed that:

- (1) Within the two-step kinetic scheme, experimental thermal curves for all the catalysts correspond most closely to the sequence of An_1 and An_2 steps, each of the steps being described by the extended Johnson–Mehl–Avrami–Erofeev–Kolmogorov (JMAEK) equation, which is known also as the Avrami–Erofeev equation:

$$[-\ln(1 - \alpha)]^{1/n} = kt \tag{4}$$

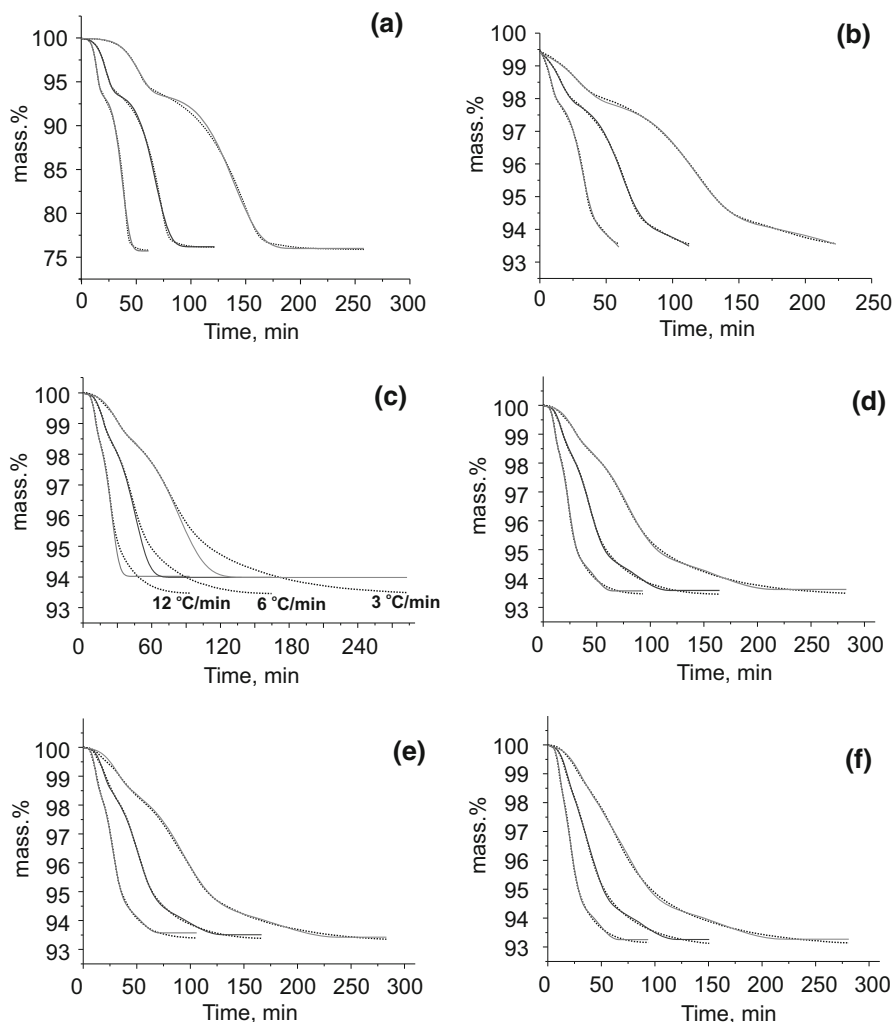


Fig. 4 A comparison of experimental TG data (*dots*) in a range from 50 to 900 °C at heating rates 3, 6 and 12 °C/min in a mixture of 50% Ar/50%H₂ and the best theoretical approximation (*lines*) of thermal reduction curves by different mechanisms: A-(An₁) → B-(An₂) → C for CoAl-M (a), CoRu(0.5)Al (c) and A-(An₁) → B-(An₂) → C-(D) → D for CoAl (b), CoRu(0.5)Al (d), CoRu(0.2)Al (e), CoRu(1.0)Al (f). An is the Avrami-Erofeev model, and D is the Jander model of 3D diffusion

The dimensional parameters n_1 and n_2 are below 1: ca. 0.5 ± 0.05 for the catalysts, and 0.6–0.7 for the model CoAl-M sample.

- (2) For the model CoAl-M sample, the JMAEK equation of An₂ adequately describes the second step (CoO* reduction) until completion of the process (Fig. 4a).

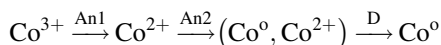
However, the inhibition of the reaction was experimentally observed for both unpromoted and ruthenium promoted catalysts upon conversion of the last 30–40%, whereas the Avrami–Erofeev equation predicts a much more sharp termination of the process (exemplified by the CoRu(0.5)Al catalyst on Fig. 4c). The experimentally observed inhibition of the reaction may indicate an impediment to the reduction process, for example, due to diffusion of reactants/products.

Indeed, when the consecutive mechanism $A \rightarrow B \rightarrow C$ was supplemented with the additional consecutive step $C \rightarrow D$, which is controlled by three-dimensional diffusion and described by the Jander equation (D):

$$\left[1 - (1 - \alpha)^{1/3} \right]^2 = kt \tag{5}$$

The kinetic parameters obtained by the An_1 and An_2 equations within the two-step scheme were fixed, the best fit of the model curves to experimental data was obtained (Figs. 4b, 4d, 4e, 4f).

Thus, a complete reduction of cobalt catalysts can be described as the consecutive process:



This kinetic scheme was used to determine the activation energy E_a , the logarithm of pre-exponential factor ($\log A$), and the fraction of the step in a complete conversion (FollReact.) at approximately similar correlation coefficients (Table 2).

One can see in Table 2 that the introduction of 0.2–0.5 wt% Ru into the catalyst decreases the activation energy of all three consecutive steps of the process; the most pronounced difference (80 kJ/mol) is observed for the final step controlled by diffusion. It should be noted that the decrease in activation energy of the first two

Table 2 Kinetic parameters of the reduction of CoAl and CoRu(x)Al catalysts determined for the kinetic scheme $A \rightarrow B \rightarrow C \rightarrow D$ that comprises two consecutive steps obeying the JMAEK equation and the third step of 3D Jander diffusion

Sample	CoAl–M	CoAl	CoRu(0.2)Al	CoRu(0.5)Al	CoRu(1.0)Al
An₁					
E_a , kJ/mol	101 ± 7	107 ± 7	102 ± 10	85 ± 7	85 ± 14
$\log A$, s ⁻¹	6.3 ± 0.7	7.7 ± 0.7	8.9 ± 1.2	8.1 ± 0.9	8.2 ± 1.8
FollReact.	0.27	0.26	0.22	0.23	0.23
An₂					
E_a , kJ/mol	134 ± 4	120 ± 5	102 ± 3	98 ± 3	90 ± 5
$\log A$, s ⁻¹	5.2 ± 0.2	4.7 ± 0.3	5.3 ± 0.2	5.7 ± 0.3	5.2 ± 0.5
FollReact.	–	0.60	0.61	0.60	0.57
D					
E_a , kJ/mol	–	186 ± 31	112 ± 12	100 ± 7	91 ± 10
$\log A$, s ⁻¹	–	4.7 ± 2	2.2 ± 0.6	1.9 ± 0.5	1.5 ± 0.6
Correlation coefficient	0.99956	0.99980	0.99963	0.99966	0.99953

kinetic steps is accompanied by an increase in pre-exponential factor. On the contrary, at the diffusion-controlled step the decrease in activation energy linearly correlates with the logarithm of pre-exponential factor:

$$\ln A = aE_a + b \quad (6)$$

It means that the so-called “kinetic compensation effect” takes place at this step. The compensation effect occurs here because the third step (D) is a chemical process the kinetics of which is complicated by mass transfer processes (the Jander model). Accordingly, the apparent activation energy and the pre-exponential factor depend on the ratio of rate constants of the chemical process and mass transfer coefficient: in the case of tough diffusion control of the process, the apparent activation energy approaches the activation energy of cobalt cations diffusion in the oxide (CoAl catalyst), while weakening of the control brings the apparent activation energy close to the activation energy of the chemical reduction of Co^{2+} (CoRu(1.0)Al catalyst). This gives rise to the correlation shown in Eq. 6 [36]. A joint decrease in the activation energy and pre-exponential factor in the course of ruthenium promotion corresponds to a weaker diffusion impediment at the final step of cobalt reduction.

The absence of compensation effect at the first two kinetic steps does not mean that mass transfer processes do not complicate their occurrence. On the contrary, nonintegral value of the n order in the Avrami–Erofeev equation may indicate that the interface propagation rate is described by the parabolic law and is proportional to $(Dt)^{0.5}$ (here, D is the diffusion coefficient); this testifies to the diffusion-controlled growth of the product nuclei [37, 38]. In this case, the 0.5 order may indicate instantaneous nucleation (or a complete coverage of the external surface of reacting phase with the compactly growing nuclei) followed by the diffusion-controlled one-dimensional growth. However, it should be mentioned that such interpretation of parameters of Eq. 4 is correct only if processes are examined under isothermal conditions. It is known that the simulation based on the data of kinetic experiments under non-isothermal conditions may give incorrect values of kinetic parameters [39, 40]. Thus, the actual mechanism can be revealed and real values of kinetic parameters can be obtained by comparing the kinetic modeling data obtained under non-isothermal conditions with the data obtained under isothermal conditions. Unfortunately, the kinetic study of the reduction of Co–Al catalysts under isothermal conditions is a difficult and unusual problem requiring big time intervals; so, we could not perform such studies under available conditions. If it is difficult or impossible to run the process under isothermal conditions, kinetic modeling data can be compared with the data acquired by isoconversional methods [40].

In our case, the values of kinetic parameters obtained by the model method for the reduction of CoRu(x)Al catalysts and CoAl–M are close to the values acquired by isoconversional methods and agree well with the published data on the reduction kinetics of bulk Co_3O_4 and supported cobalt catalysts under non-isothermal conditions [41–45]. However, some authors proposed other kinetic models describing the process of cobalt reduction. In [41], kinetic dependences obtained

by TG method were used to describe both steps of Co_3O_4 reduction in a pure hydrogen medium by the model of autocatalytic reaction using the extended Prout–Tompkins equation:

$$\frac{d\alpha}{dt} = A \exp\left(-\frac{E_a}{RT}\right) \alpha^m (1 - \alpha)^n \quad (7)$$

The values $E_a \sim 87$ kJ/mol and $\log A = 6.2$ were used. In the indicated work, the mechanism is represented by two consecutive (parallel, according to the authors) reactions with a 88% completeness of the second step. Unfortunately, the authors did not reveal the physical meaning of parameters m and n in the Prout–Tompkins equation ($m_1 = 0.068$, $n_1 = 0.151$ and $m_2 = 0.94$, $n_2 = 0.928$).

The reduction kinetics of Co/SiO₂ catalysts was investigated by TPR and TG methods in [43, 45]. In [43], the first step of the reduction process was described by a model of two-dimensional nucleation using the Avrami–Erofeev equation with apparent $E_a = 94.4$ kJ/mol, while for the second step a model of the first order monomolecular reaction with apparent $E_a = 82.9$ kJ/mol was proposed. The authors of [45] described the first step of reduction by the Avrami–Erofeev model with $n = 1.5$ and $E_a = 104$ kJ/mol, and the second step—by the second order equation with $E_a = 118$ kJ/mol.

The analysis of the reduction kinetics of cobalt–alumina catalysts is reported in [41, 44]. Ji and co-authors [42] estimated E_a values for two steps of the reduction of Co(15%)–Al₂O₃ catalyst using the model free Kissinger method and H₂-TPR data (10% H₂/Ar). The activation energy was found to be 90 and 95 kJ/mol, respectively. In [44], the Kissinger method was applied to the data on spontaneous magnetization measured at three heating rates in 100% hydrogen. The activation energy for the formation of metallic cobalt phase was estimated as 130 kJ/mol for Co/Al₂O₃; the introduction of Pt (1 wt%) was shown to decrease the apparent E_a to 60 kJ/mol.

A comparison of thermal analysis and in situ X-ray diffraction data. Evolution of CSR sizes of cobalt-containing phases during reductive activation

All theoretical kinetic models are based on some assumptions (for example, particles of the reacting phase have similar shape and size) and/or do not take into account the possible occurrence of other processes (for example, the reduction of Co_3O_4 to CoO is accompanied by a weight loss caused by the removal of water and adsorbed ions). So, when discussing the mechanism of cobalt reduction, thermal analysis data should be considered together with the data obtained by other methods, such as in situ TEM, in situ XRD or in situ XANES.

Crystallochemical concepts of the reduction of pure Co_3O_4 are reported in [5, 6]. TEM experiments showed that the growth of CoO occurred in an epitaxial manner on Co_3O_4 with CoO(111) planes parallel to Co_3O_4 (111) planes [5]. At the next stage, CoO was reduced to Co and again epitaxial growth with Co(111) parallel to CoO(111) was observed. It was found also that the particles with the size of ca. 5 nm and rounded shape have more structural defects and are completely reduced to

the metal at 300 °C in a 100% hydrogen medium, whereas the particles larger than 12 nm that are represented by well crystallized polyhedra are reduced incompletely and have oxidized cobalt species Co_3O_4 and CoO . As the reduction temperature of Co_3O_4 with the particle size of 12 nm and larger is raised, a relative amount of CoO decreases, and the particles reduced at 500 °C have only the Co_3O_4 and Co phases. Thus, the authors suppose that the reduction of CoO to Co is the autocatalytic process. In [6], the in situ TEM study revealed that at a hydrogen pressure of 0.1 mbar the reduction of Co_3O_4 to CoO proceeds via the formation of an advancing atomic scale interface between Co_3O_4 and CoO regions. The interface penetrates further into the Co_3O_4 crystal, with the CoO regions replacing the previous Co_3O_4 structure, with increasing reduction. The reduction to CoO proceeds at approximately 200 °C at rounded edges containing atomic steps on the surfaces. A temperature of 450 °C was required to reduce CoO to the metal at a hydrogen pressure of 3 mbar. In the process, Co metal forms small clusters on the crystals and eventually spreads, forming a Co shell.

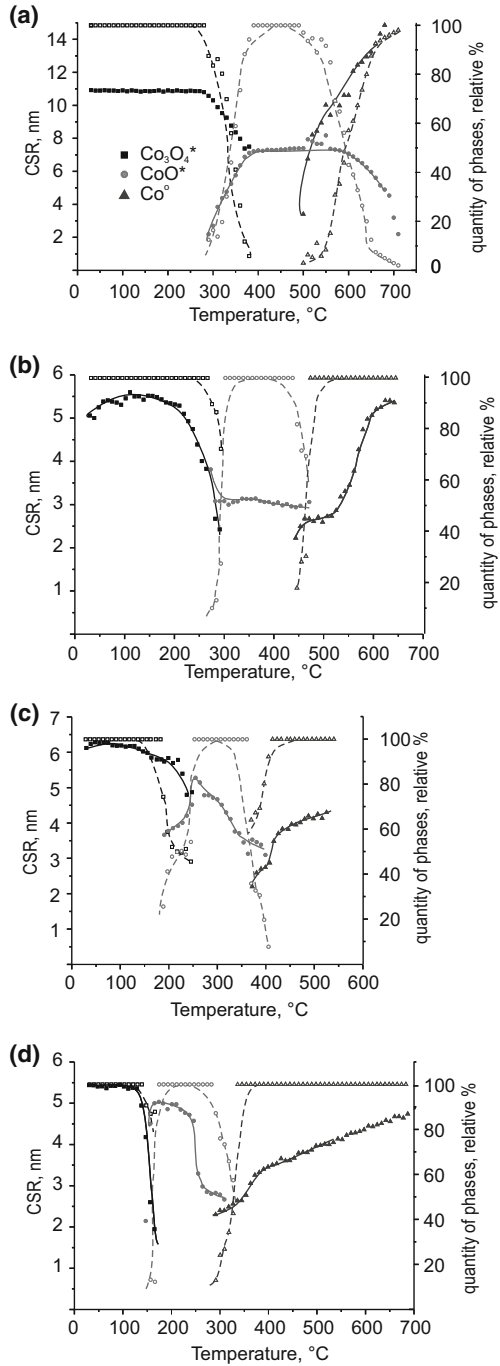
In [2, 13, 46, 47], the reduction of supported cobalt-containing systems was studied by in situ XRD in a 100% hydrogen medium. The reduction of bulk Co_3O_4 having a defect spinel structure proceeds in the region of 350–400 °C and results in the formation of the metallic phase with the hcp structure. In supported systems, the initial Co_3O_4 spinel phase has a defect structure due to interaction with the support and is reduced at higher temperatures. Therewith, the metallic phase is present mostly as the fcc structure [2, 13]. A recent temperature differential ferromagnetic nuclear resonance study [48] showed that metallic particles with the size of 3–10 nm in carbon-supported cobalt systems are represented predominantly by the hcp structure and are most active in FTS. Accordingly, larger particles have mostly the fcc structure.

In situ XRD data allow estimating the evolution of CSR sizes of cobalt-containing oxides and metallic cobalt in the observed consecutive chemical reactions $\text{Co}_3\text{O}_4^* \rightarrow \text{CoO}^*$ and $\text{CoO}^* \rightarrow \text{Co}^0$.

Fig. 5 shows experimentally estimated CSR sizes of cobalt-containing phases in the tested catalyst samples and model CoAl-M sample versus the reduction temperature.

As seen on Fig. 5, the dependences of average CSR sizes on the reduction temperature for the model sample and supported unmodified catalyst are quite similar but differ from that of ruthenium promoted catalysts. For all the samples, the initial CSR sizes of the Co_3O_4^* phase are in the range of 5–11 nm. For the model sample, the average CSR sizes of the initial Co_3O_4^* phase are somewhat higher as compared to the supported unmodified catalyst, which may be caused by the formation of the cobalt oxide precursor (hydrotalcite) during precipitation in the free volume of solution rather than on the support surface. The introduction of ruthenium into the catalyst increased the CSR sizes of the initial oxide phase; however, the CSR size of the metallic cobalt phase formed at 400–500 °C was somewhat lower as compared to unmodified catalyst: 4–5 nm against 6–7 nm. This verifies the earlier reported observations indicating that ruthenium promotion increases the dispersion of metallic cobalt particles [14–20].

Fig. 5 Dependences of experimentally estimated CSR sizes (*shaded symbols* left ordinate) and relative amount of the phase of cobalt-containing phases (*hollow symbols* right ordinate) on the reduction temperature which were obtained in situ upon reduction in 100% hydrogen at a heating rate of 3 °C/min: **a** CoAl–M, **b** CoAl, **c** CoRu(0.2)Al, **d** CoRu(1.0)Al



At the first reduction step (for CoAl catalyst, this is the temperature range of 150–400 °C), the $(\text{Co}, \text{Al})_3\text{O}_4$ spinel-like phase transforms into the CoO^* oxide phase having the NaCl-like structure. Changes in the intensity of diffraction lines corresponding to the $(\text{Co}, \text{Al})_3\text{O}_4$ phase are accompanied by their broadening, which testifies to a decrease in the observed CSR size. This may be caused by both the decrease in the particle diameter of the phase (in some cases, the CSR size is an adequate estimate of the particle diameter) and the increase in the concentration of defects in $(\text{Co}, \text{Al})_3\text{O}_4$ oxide particles. The initial CSR size of the $(\text{Co}, \text{Al})_3\text{O}_4$ phase in CoAl catalyst is ca. 6.6 nm. Just before the disappearance of diffraction maxima of this phase from diffraction pattern of the catalyst in the region of 350 °C, the CSR size can be estimated as 2.7 nm. Evidently, the diffraction maxima of the $(\text{Co}, \text{Al})_3\text{O}_4$ phase cannot be identified at higher temperatures due to their low intensity and large width. It seems reasonable to suppose that the transformation of the $(\text{Co}, \text{Al})_3\text{O}_4$ phase was accompanied by a monotonous decrease in the particle sizes of the phase until a complete disappearance of the particles.

Along with decreasing the amount of the $(\text{Co}, \text{Al})_3\text{O}_4$ phase, the appearance of reflections from the CoO^* phase is observed; an increase in intensity of the diffraction maxima of CoO^* is accompanied by narrowing of the lines. In the region of ca. 340 °C, where the conversion of $(\text{Co}, \text{Al})_3\text{O}_4$ to CoO^* is close to completion, the CSR size of CoO^* is ca. 3.8 nm.

A comparison of the dynamics of decreasing the CSR size with the dynamics of a simultaneous decrease in the amount of $(\text{Co}, \text{Al})_3\text{O}_4$ phase showed that the CSR shape did not remain constant in the process. Thus, at 280 °C the CSR size of $(\text{Co}, \text{Al})_3\text{O}_4$ is ca. 3.0 nm. Assuming a constant CSR shape, this 45% decrease in its size corresponds to a sixfold decrease in the volume ($V \propto d^3$); however, data on the intensity of X-ray diffraction lines indicate that at this moment only ca. 50% of the $(\text{Co}, \text{Al})_3\text{O}_4$ oxide was converted to CoO^* . Hence, it should be supposed that the process of cobalt reduction and $(\text{Co}, \text{Al})_3\text{O}_4$ transformation to CoO^* is accompanied by the formation of several nuclei in the oxide particle. This agrees with the results of modeling the process kinetics by regression analysis methods—the best description of the process is obtained with the JMAEK equation.

The molar volume of Co_3O_4 oxide is $22.0 \text{ \AA}^3/\text{at}_{\text{Co}}$ or $1.33 \times 10^{-5} \text{ m}^3/\text{mol}_{\text{Co}}$ (PDF#421467). Accordingly, a CSR with the size of 5.5 nm contains ca. $7.9 \times 10^{-19} \text{ mol Co}$ (approximately 7500 atoms). (For definiteness, the cubic shape of CSR was assumed; this is not essential for further reasoning). After the reduction to CoO oxide (the molar volume of $19.2 \text{ \AA}^3/\text{at}_{\text{Co}}$ or $1.16 \times 10^{-5} \text{ m}^3/\text{mol}_{\text{Co}}$, PDF#431004), the cobalt amount indicated above will fill the 144 nm^3 volume, which corresponds to the size of 5.2 nm with the retained CSR shape. The experimentally observed CSR size of the CoO phase is 3.0 nm, and volume of one CSR with such a size will be ca. 27 nm^3 under the assumption of the same cubic shape; hence, after the reduction to CoO^* , cobalt oxide that constituted one CSR of the initial Co_3O_4 phase transforms into several (in this case at least into five) coherent scattering regions of the new phase. This suggests that at least a part of Al^{3+} cations of the initial spinel-like oxide, the presence of which in the CoO^* phase is possible only due to violation of the oxide stoichiometry, is displaced to the interdomain boundary, i.e. to the surface of the growing CoO^* particle.

Accordingly, upon the completion of the reduction, Al^{3+} cations are located at the interdomain boundary and stabilize such a small size of the domain (CSR) of CoO^* oxide. The above discussed features of the first reduction step are as well typical of the model sample. The initial observed CSR size of $(\text{Co}, \text{Al})_3\text{O}_4$ phase was 11 nm, and the CSR size of form CoO^* was 7.7 nm. Assuming the similarity of the CSR shape, one CSR of Co_3O_4^* is converted into 3 CSR of CoO^* . The ruthenium promotion of catalyst has a significant impact on the Co_3O_4^* reduction process and leads to significantly fewer crystallites CoO^* from the original spinel-like oxide phase. Thus, one CSR of $(\text{Co}, \text{Al})_3\text{O}_4$ transforms into 2 and 1 CSR of CoO^* for $\text{CoRu}(0.2)\text{Al}$ at 260 °C and for $\text{CoRu}(1.0)\text{Al}$ at 160 °C, correspondingly.

The second reduction step, which relates to the formation of metallic cobalt particles, takes place in the temperature range above 340 °C for the CoAl catalyst. However, the width of the CoO^* phase diffraction lines remains almost unchanged until their disappearance at 470 °C, the corresponding CSR size of CoO^* is 2.9–3.0 nm. The metallic cobalt phase can be identified on diffraction patterns only at above 445 °C with CSR ca. 2.5 nm, despite the fact that only about 30% of the CoO^* phase transformed into metal at 460 °C. The absence of any dynamics of CSR size of oxide CoO^* and simultaneous coexistence of phases CoO^* and Co^0 may indicate that the reduction of cobalt oxide is limited by the step of metallic phase nucleation: after the emergence of the Co^0 nucleus, further transformation of the entire particle (CSR) of CoO^* proceeds rapidly. Each CSR of CoO^* transforms into 1 CSR of Co^0 , note, that CSR of the metallic cobalt was still below 2.6 nm at 530 °C, when the phase of CoO^* was not recorded already.

A further temperature elevation results in a twofold increase in CSR size of metallic cobalt that is most likely due to the coalescence of a few neighboring metal particles. The coalescence of metallic particles is expected, since CoAl catalyst reduction occurs at temperatures above the Tammann temperature of metallic cobalt ($T_T \approx \frac{1}{2} T_m \approx 880 \text{ K}$).

Unlike unpromoted CoAl catalyst, Ru-promoted samples exhibit significant decrease in CoO^* CSR size just before the metallic phase was detected: in $\text{CoRu}(0.2)\text{Al}$ CSR of CoO^* decreased from 5 to 3.5 nm at 350 °C, and in $\text{CoRu}(1.0)\text{Al}$ to 2.7 nm at 250 °C. After the emergence of the metallic phase, the further diminishing of CoO^* CSR size is slowing, which can be seen as a «step» at the corresponding plot in Fig. 5. The CSR of metallic phase is gradually increasing from 2.2–2.3 nm up to 4–4.5 nm with another «step» near the temperature of CoO^* phase vanishing. The final CSR of Co^0 (at above 500 °C) matches well the stoichiometry of 1 CoO^* CSR transforming to 1 metallic Co CSR. All these observations fit to the JAEMK model of the new phase nucleation, nuclei growth and further coalescence. It is noteworthy that a similar evolution of CSR sizes of cobalt-containing phases upon the reduction was observed of the 22% wt. Co–Al catalyst prepared by deposition of Co ammonia complex [49].

Data of kinetic modeling indicate that the best description of thermal analysis curves is obtained under the assumption that the An_2 process is followed by a three-dimensional diffusion-controlled process according to the Jander model. Kinetic limitations by diffusion of the reduction of CoO^* oxide after reaching a 50% conversion agree well with the slow growth of CSR size of Co^0 particles after step-

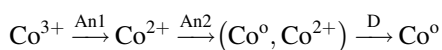
like growth (see Fig. 5c, d). Therefore, the reduction of the CoO* phase should be described as nucleation of the metallic cobalt phase with the size of crystallites ca. 2 nm in the oxide particle, their growth and coalescence to a size of about 3.5 nm, and the subsequent growth of the metal particles which is kinetically limited by diffusion of ions through the 1–2 nm thick layer of Co–Al oxide. The 1–2 nm layer of the oxide can't be detected by X-ray diffraction.

Conclusions

The TG and in situ XRD study of cobalt–alumina systems promoted with ruthenium from *trans*-Ru(NO)(NH₃)₂(NO₃)₃ complex under the conditions of temperature-programmed heating in a hydrogen-containing medium made it possible to reveal the effect of ruthenium on the cobalt reduction in flowing hydrogen, estimate kinetic parameters and discuss the distinctive features of the cobalt reduction mechanism.

Upon reductive treatment, the Co₃O₄* cobalt oxide phase (an asterisk indicates the possible presence of aluminum cations in the oxide) successively transforms into CoO* oxide and metallic cobalt. The introduction of small amounts of ruthenium (up to 1 wt%) from *trans*-Ru(NO)(NH₃)₂(NO₃)₃ complex accelerates the reduction process and decreases the characteristic temperatures of both reduction steps (Co³⁺ → Co²⁺ and Co²⁺ → Co⁰). Therewith, the temperature range in which the metallic cobalt phase is formed shifts to lower temperatures by more than 250 °C. Results of the model free analysis by the Friedman and Ozawa–Flynn–Wall isoconventional methods indicated a considerable (ca. 25–40%) decrease in the apparent E_a of both reduction steps for the promoted systems.

Modeling of experimental kinetic dependences by regression analysis methods and estimation of evolution of the size of coherent scattering regions for cobalt-containing phases showed that the reduction of ruthenium promoted Co/δ-Al₂O₃ catalysts is sequential and consists of three steps:



The first step proceeds through the formation of several CoO* phase centers (including CoO) within one Co₃O₄* crystallite and is followed by their further growth, which is described by the JMAEK kinetic model (An₁) with n₁ < 1, which may indicate significant diffusion constraints of the CoO* nuclei growth. Several nuclei of the CoO* phase form several discrete domains from one Co₃O₄* crystallite. Stabilization of the highly disperse state of CoO* may be provided by aluminum cations that constituted the initial Co₃O₄* and were displaced to the interdomain boundary in the course of reduction. Ruthenium promotion of the catalyst leads to significantly fewer crystallites CoO* from the initial spinel-like oxide phase. For the 1% Ru-promoted catalyst, one has to suppose that each CSR of Co₃O₄* transforms into 1 CSR of CoO*.

The second step is a kinetically controlled sequential process of the Co metal phase nucleation (An₂) followed by the step of slow particle growth, which is limited by the diffusion of ions in the oxide according to the Jander model (D). At

step D, ruthenium promotion produces a joint decrease in the values of apparent activation energy and pre-exponential factor (obeying the linear expression of isokinetic (compensation) effect), which testifies that diffusion limitations become weaker at the final step of cobalt reduction. In the case of unmodified Co/ δ -Al₂O₃, the characteristic temperature of the metal phase formation reaches very high values at which the metal nuclei rapidly coalesce into larger ones. For ruthenium promoted catalysts, each CoO* crystallite generates one metal crystallite; thus, ruthenium enhances the dispersion of the active component at relatively low temperatures.

Acknowledgements The research was supported by the joint Research and Educational Center for Energy Efficient Catalysis (Novosibirsk State University and Borekov Institute of Catalysis SB RAS), by Russian Government Decree No. V.45.3.6. The authors are grateful to Prof. V.A. Emelyanov (Novosibirsk State University) who afforded *trans*-Ru(NO)(NH₃)₂(NO₃)₃ complex for the study and Dr. I.I. Simentsova who afforded Co–Al–M sample for the study.

References

1. Jacobs G, Ji Y, Davis BH, Cronauer D, Kropf AJ, Marshall ChL (2007) Fischer-Tropsch synthesis: temperature programmed EXAFS/XANES investigation of the influence of support type, cobalt loading and noble metal promoter addition to the reduction behavior of cobalt oxide particles. *Appl Catal A* 333:177–191
2. Bulavchenko OA, Cherepanova SV, Malakhov VV, Dovlitova LS, Ishchenko AV, Tsybulya SV (2009) In situ XRD study of nanocrystalline cobalt oxide reduction. *Kinet Catal* 50:192–198
3. Simentsova II, Khassin AA, Minyukova TP, Davydova LP, Shmakov AN, Bulavchenko OA, Cherepanova SV, Kustova GN, Yurieva TM (2012) The effect of composition and structure of a precursor compound on the catalytic properties of cobalt-aluminum catalysts in Fischer-Tropsch reactions. *Kinet Catal* 53(4):520–526
4. Hong J, Marceau E, Khodakov AYU, Gaberová L, Griboval-Constant A, Girardon JS, La Fontaine C, Briois V (2015) Speciation of ruthenium as a reduction promoter of silica-supported Co catalysts: a time-resolved in situ XAS investigation. *ACS Catal* 5:1273–1282
5. Potoczna-Petru D, Kępiński L (2001) Reduction study of Co₃O₄ model catalyst by electron microscopy. *Catal Lett* 73:41–46
6. Ward MR, Boyes ED, Gai PL (2013) In situ aberration-corrected environmental TEM: reduction of model Co₃O₄ in H₂ at the atomic level. *ChemCatChem* 5:2655–2661
7. Reueland R, Bartholomew CH (1984) Effects of support and dispersion on the CO hydrogenation activity/selectivity properties of cobalt. *J Catal* 85:78–88
8. Arnoldy P, Moulijn JA (1985) Temperature-programmed reduction of CoO/Al₂O₃ catalysts. *J Catal* 93:38–54
9. Hansteen OH, Fjellvag H, Hauback BC (1998) Reduction, Crystal Structure and Magnetic Properties of Co_{0(3-x)Al_xO_(4-delta)} (0.0 ≤ X ≤ 2.0, 0.0 ≤ delta ≤ 1.0). Comparison with the Co/gamma-Al₂O₃ Fischer-Tropsch catalyst. *Acta Chem Scand* 52:1285–1292
10. Khassin AA, Anufrienko VF, Ikorskii VN, Plyasova LM, Kustova GN, Larina TV, Molina IYu, Parmon VN (2002) Physico-chemical study on the state of cobalt in a precipitated cobalt-aluminum oxide system. *Phys Chem Chem Phys* 4:4236–4243
11. Tsakoumis NE, Rønning M, Borg Ø, Rytter E, Holmen A (2010) Deactivation of cobalt based Fischer-Tropsch catalysts: a review. *Catal Today* 154:162–182
12. Jacobs G, Sarkar A, Ji Y, Luo M, Dozier A, Davis BH (2008) Fischer-Tropsch synthesis: assessment of the ripening of cobalt clusters and mixing between Co and Ru Promoter via oxidation–reduction-cycles over lower Co-loaded Ru–Co/Al₂O₃ catalysts. *Ind En Chem Res* 47(3):672–680
13. Khodakov AYU, Lynch J, Bazin D, Rebours B, Zanier N, Moisson B, Chaumette P (1997) Reducibility of cobalt species in silica-supported Fischer-Tropsch catalysts. *J Catal* 168:16–25
14. Tsubaki N, Sun S, Fujimoto K (2001) Different functions of the noble metals added to cobalt catalysts for Fischer-Tropsch synthesis. *J Catal* 199:236–246

15. Ma W, Jacobs G, Keogh RA, Bukur DB, Davis BH (2012) Fischer-Tropsch synthesis: effect of Pd, Pt, Re, and Ru noble metal promoters on the activity and selectivity of a 25%Co/Al₂O₃ catalyst. *Appl Catal A* 437–438:1–9
16. Jacobs G, Patterson PM, Zhang Y, Das T, Li J, Davis BH (2002) Fischer-Tropsch synthesis: deactivation of noble metal-promoted Co/Al₂O₃ catalysts. *Appl Catal A* 233:263–281
17. Song S-H, Lee S-B, Bae JW, Sai Prasad PS, Jun K-W (2008) Influence of Ru segregation on the activity of Ru-Co/ γ -Al₂O₃ during FT synthesis: a comparison with that of Ru-Co/SiO₂ catalysts. *Catal Commun* 9:2282–2286
18. Kogelbauer A, Goodwin JG Jr, Oukaci R (1996) Ruthenium promotion of Co/Al₂O₃ Fischer Tropsch catalysts. *J Catal* 160:125–133
19. Park J-Y, Lee Y-J, Karandikar PR, Jun K-W, Bae JW, Ha K-S (2011) Ru promoted cobalt catalyst on γ -Al₂O₃ support: influence of pre-synthesized nanoparticles on Fischer-Tropsch reaction. *J Mol Catal A* 344:153–160
20. Parnian MJ, Najafabadi AT, Mortazavi Y, Khodadadi AA, Nazzari I (2014) Ru promoted cobalt catalyst on γ -Al₂O₃: influence of different catalyst preparation method and Ru loadings on Fischer-Tropsch reaction and kinetics. *Appl Surf Sci* 313:183–195
21. Cook KM, Poudyal S, Miller JT, Bartholomew CH, Hecker WC (2012) Reducibility of alumina-supported cobalt Fischer-Tropsch catalysts: effects of noble metal type, distribution, retention, chemical state, bonding, and influence on cobalt crystallite size. *Appl Catal A* 449:69–80
22. Hilmen AM, Schanke D, Holmen A (1996) TPR study of the mechanism of rhenium promotion of alumina-supported cobalt Fischer-Tropsch catalysts. *Catal Lett* 38:143–147
23. Nabaho D, Niemantsverdriet JW, Claeys M, van Steen E (2016) Hydrogen spillover in the Fischer-Tropsch synthesis: an analysis of platinum as a promoter for cobalt–alumina catalysts. *Catal Today* 261:17–27
24. Beaumont SK, Alayoglu S, Specht C, Michalak WD, Pushkarev VV, Guo J, Kruse N, Somorjai GA (2014) Combining in situ NEXAFS spectroscopy and CO₂ methanation kinetics to study Pt and Co nanoparticle catalysts reveals key insights into the role of platinum in promoted cobalt catalysis. *J Am Chem Soc* 136:9898–9901
25. Jacobs G, Chaney JA, Patterson PM, Das TK, Maillot JC, Davis BH (2004) Fischer-Tropsch synthesis: study of the promotion of Pt on the reduction property of Co/Al₂O₃ catalysts by in situ EXAFS of Co K and Pt LIII edges and XPS. *J Synchrotron Radiat* 11:414–422
26. Iglesia E, Soled SL, Fiato RA, Via GH (1993) Bimetallic synergy in cobalt ruthenium Fischer-Tropsch synthesis catalysts. *J Catal* 143:345–368
27. Li P, Liu J, Nag N, Crozier PA (2006) In situ synthesis and characterization of Ru promoted Co/Al₂O₃ Fischer-Tropsch catalysts. *Appl Catal A* 307:212–221
28. Geus JW, van Dillen AJ (2008) In: Ertl G, Knözinger H, Schüth F, Weitkamp J (eds) *Handbook of heterogeneous catalysis*, 2nd edn. Wiley, New York
29. Simentsova II, Khassin AA, Filonenko GA, Chermashentseva GK, Bulavchenko OA, Cherepanova SV, Yurieva TM (2011) Anionic composition of precursors of the CO/Al₂O₃ catalysts for the Fischer-Tropsch synthesis. *Russ Chem Bull* 60:1827–1834
30. Khassin AA, Simentsova II, Cherepanova SV, Shmakov AN, Shtertser NV, Bulavchenko OA (2016) Effect of nitric oxide on the formation of cobalt–aluminum oxide structure from layered double hydroxide and its further transformation during reductive activation. *Appl Catal A* 514:114–125
31. Kabin EV, Emel'yanov VA, Alferova NI, Tkachev SV, Baidina IA, Vorob'yev VA (2012) Reaction of *trans*-[RuNO(NH₃)₄(OH)]Cl₂ with nitric acid and synthesis of ammine(nitrate)nitrosoruthenium complex. *Russ J Inorg Chem* 57:1146–1153
32. Le Bail A (2005) Whole powder pattern decomposition methods and applications: a retrospective. *Powder Diffr* 20:316–326
33. Friedman HL (1969) New methods for evaluating kinetic parameters from thermal analysis data. *J Polym Sci Part B* 7:41–46
34. Ozawa T (1965) A new method of analyzing thermogravimetric data. *Bull Chem Soc Jpn* 38:1881–1886
35. Flynn J, Wall LA (1966) A quick, direct method for the determination of activation energy from thermogravimetric data. *J Polym Sci Part B* 4:323–328
36. Vyazovkin SV (2003) Model-free kinetics. *J Therm Anal Calorim* 83:45–51
37. Sun NX, Liu XD, Lu K (1996) An explanation to the anomalous Avrami exponent. *Scr Mater* 34:1201–1207

38. Brown ME, Dollimore D, Galwey AK (1980) In: Bamford CH, Tipper CFH (eds) *Comprehensive chemical kinetics*. Elsevier, Amsterdam
39. De Bruijn TJW, De Jong WA, Van Den Berg PJ (1981) Kinetic parameters in Avrami–Erofeev type reactions from isothermal and non-isothermal experiments. *Thermochim Acta* 45:315–325
40. Vyazovkin S, Wigh CA (1997) Isothermal and nonisothermal reaction kinetics in solids: in search of ways toward consensus. *J Phys Chem A* 101:8279–8284
41. Tomic-Tucakovic B, Majstorovic D, Jelic D, Mentus S (2012) Thermogravimetric study of the kinetics of Co_3O_4 reduction by hydrogen. *Thermochim Acta* 541:15–24
42. Ji Y, Zhao Zh, Duan A, Jiang G, Liu J (2009) Comparative study on the formation and reduction of bulk and Al_2O_3 -supported cobalt oxides by H_2 -TPR technique. *J Phys Chem C* 113:7186–7199
43. Lin H-Y, Chen Y-W (2007) The mechanism of reduction of cobalt by hydrogen. *Mater Chem Phys* 85:171–175
44. Chu W, Chernavskii PA, Gengembre L, Pankina GA, Fongarland P, Khodakov AY (2007) Cobalt species in promoted cobalt alumina-supported Fischer-Tropsch catalysts. *J Catal* 252:215–230
45. Wan YJ, Li JL, Chen DH (2007) Kinetic characterization of the reduction of silica supported cobalt catalysts. *J Therm Anal Calorim* 90:415–419
46. Garces LJ, Hincapie B, Zerger R, Suib SL (2015) The effect of temperature and support on the reduction of cobalt oxide: an in situ X-ray diffraction study. *J Phys Chem C* 119(10):5484–5490
47. Smith ML, Campos A, Spivey JJ (2012) Reduction processes in Cu/SiO_2 , Co/SiO_2 , and CuCo/SiO_2 catalysts. *Catal Today* 182(1):60–66
48. Liu Y, Luo J, Shin Y, Moldovan S, Ersen O, Hebraud A, Schlatter G, Pham-Huu C, Meny Ch (2016) Sampling the structure and chemical order in assemblies of ferromagnetic nanoparticles by nuclear magnetic resonance. *Nat Commun*. doi:[10.1038/ncomms115327](https://doi.org/10.1038/ncomms115327)
49. Lok CM (2004) Novel highly dispersed cobalt catalysts for improved Fischer-Tropsch productivity. *Stud Surf Sci Catal* 147:283–288